NUMERICAL SIMULATIONS AND LABORATORY MEASUREMENTS IN HYDRAULIC JUMPS

LUIS G. CASTILLO, JOSÉ M. CARRILLO, JUAN T. GARCÍA, ANTONIO VIGUERAS-RODRÍGUEZ
Hidr@mGroup, Department of Civil Engineering, Universidad Politécnica de Cartagena,
Paseo Alfonso XIII, 52, 30203, Cartagena, Spain, email: luis.castillo@upct.es;
jose.carrillo@upct.es; juan.gbermejo@upct.es; avigueras.rodriguez@upct.es

Hydraulic jump is one of the most extended and effective mechanism for hydraulic energy dissipation. Usually, hydraulic jump characteristics have been studied through physical models. Nowadays, computational fluid dynamics (CFD) are an important tool that can help to analyze and to understand complex phenomena that involve high turbulence and air entrainment cases. Free and submerged hydraulic jumps are studied in a rectangular channel downstream a sluice gate. Velocity measurements are carried out by using an Acoustic Doppler Velocimeter (ADV) and a Particle Image Velocimeter (PIV). The CFD models boundary conditions are based on laboratory measurements. Air-water two-phase flows are considered in the simulations. The closure problem is solved by using a two-equations turbulence model. Water depths, hydraulic jumps lengths and velocity profiles are compared with laboratory measurements.

INTRODUCTION

The Computational Fluid Dynamics programs can simulate the interaction among different fluids as a two-phase air-water flow. The programs solve the fluid mechanic problem into any geometric configuration, providing a large amount of data in the fluid domain, acceptable reliability and reduced simulation times than that obtained with experimental procedures. However, it is necessary to validate numerical models with the data obtained in prototypes or physic models.

Experimental data measured in the laboratory was used in order to establish the boundary conditions in the following two commercial CFD programs ANSYS CFX v.14.0 [1] and FLOW-3D v10.0 [6], and the Open Source program OpenFOAM v2.2.2 [11].

For the turbulent flow, CFD codes solve the differential Reynolds-Averaged Navier-Stokes (RANS) equations in the fluid domain, retaining the reference quantity in the three directions for each control volume identified. The equations for conservation of mass and momentum for incompressible flow may be written as:

$$\frac{\partial U_j}{\partial x_j} = 0 \tag{1}$$

$$\frac{\partial \rho U_i}{\partial t} + \frac{\partial}{\partial x_j}(\rho U_i U_j) = -\frac{\partial p}{\partial x_i} + \frac{\partial}{\partial x_j}(2\mu S_{ij} - \rho\overline{u_i' u_j'}) \qquad (2)$$

where i and j are indexes, x_i represents the coordinates (i = 1 to 3 for x, y, z directions, respectively), ρ the density, t the time, U the velocity vector, p the pressure, u_i' presents the turbulent velocity in each direction (i= 1 to 3 for x, y, z directions, respectively), μ is the molecular viscosity, S_{ij} is the mean strain-rate tensor and $-\rho\overline{u_i' u_j'}$ is the Reynolds stress.

Eddy-viscosity turbulence models consider that such turbulence consists of small eddies which are continuously forming and dissipating, and in which the Reynolds stresses are assumed to be proportional to mean velocity gradients. The Reynolds stresses may be related to the mean velocity gradients and eddy viscosity by the gradient diffusion hypothesis:

$$-\rho\overline{u_i' u_j'} = \mu_t\left(\frac{\partial U_i}{\partial x_j} + \frac{\partial U_j}{\partial x_i}\right) - \frac{2}{3}\delta_{ij}\rho k \qquad (3)$$

with μ_t being the eddy viscosity or turbulent viscosity, $k = \frac{1}{2}\overline{u_i' u_i'}$ the turbulent kinetic energy and δ the Kronecker delta function.

LABORATORY MODEL

Free and submerged hydraulic jumps are obtained in a channel of the Hydraulic Laboratory at the Universidad Politécnica de Cartagena. The channel is 5-meter long and 0.083-meter wide. The hydraulic jumps were obtained downstream of a sluice gate (Figure 1).
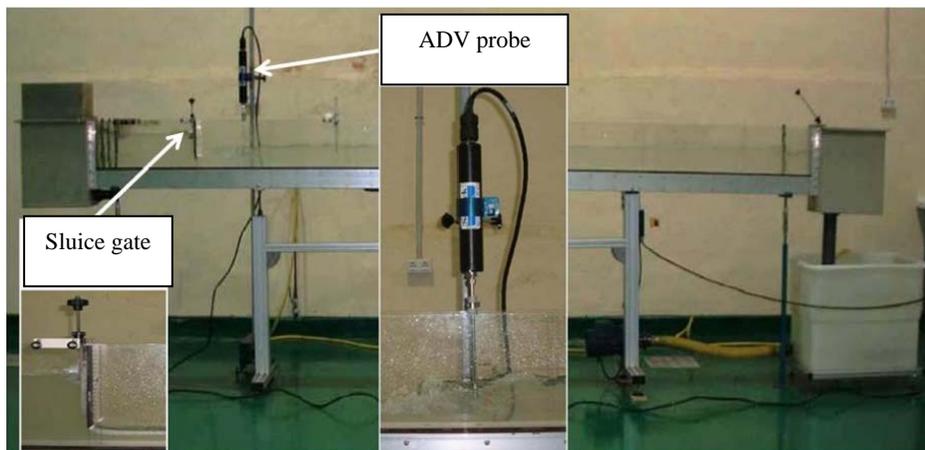

Figure 1. Free hydraulic jump at laboratory and acoustic Doppler velocimeter

An acoustic Doppler velocimeter (ADV) 10MHz of Nortek As [10] was used to measure the instantaneous velocity in three directions. The velocity range of ±100 cm/s and a 6 mm sample volume were selected. With this setting, the accuracy of the velocity measurements is ±1%. It was used a sample rate of 10 Hz with a total of 4000 measures per point. The data filtering was based on a register progressive cut of the lower and upper limits, in function of the 5% and 95% statistical (Castillo [2], [3]).

A Particle Image Velocimetry (PIV) from Etalon Research Ltd. [5] was used. This equipment allow to capture up to 16 Hz image-pair, with an adjustable laser/camera timing synchronizer. Distance from camera to channel is about 1.3 m. Values of laser pulse (dt) used are between 0.7 and 1.8 ms and the duration time between laser pulse (Dt) varies from 2.5 to 3.8 ms. With this setting, results are obtained with a frequency of 10 hz. Samples of 4000 registers have been taken for each section measured. Subwindow size is of 16x16 pixel with an overlap of 50%.

Figure 2. PIV instrumentation position and detail of post processing velocity vectors

A cross correlation algorithm was used to determine the velocity vectors with an accuracy of 0.1 pixel. The camera multi-pass correlation from 64x64 subwindow was chosen. The data filtering is based on a register progressive cut of the lower and upper limits, as a function of the 5% and 95% statistical.

Table 1 shows the characteristics of the hydraulic jumps tested, where y_1 is the initial (supercritical) depth, V_1 the horizontal velocity corresponding to the supercritical depth, y_2 the depth at the end of the hydraulic jump, y_3 the depth downstream the sluice in the submerged jump case, y_4 the depth downstream the submerged jump, and L the length of the hydraulic jump measured in the lab.

Table 1. Characteristics of the free and submerged hydraulic jumps

Type	Flow rate (m^3/s)	Sluice opening (m)	$y_1 - y_3$ (m)	V_1 (m/s)	$y_2 - y_4$ (m)	L (m)	Froude number
Free	0.0030	0.039	0.026	0.013	0.092	0.049	2.69
Submerged	0.0030	0.039	0.068	0.013	0.109	0.055	1.80

NUMERICAL MODEL

Among the different models of turbulence that complements the RANS equations, the two-equation models has been widely applied in the solution of many flows of engineering interest. ANSYS CFX and OpenFOAM allow to use two-equation turbulence models based in k-ε and in k-ω. However, FLOW-3D only allows to use two-equation turbulence models based in k-ε. In order to have a better knowledge of the numerical results, the k-ε model (Harlow and Nakayama [7], Launder and Sharma [9]) has been selected in the three CFD codes, so that results can be

compared. This model is implemented in most general purpose CFD codes and is considered the industry standard model. The effective viscosity is calculated as:

$$\mu_t = C_\mu \rho \frac{k^2}{\varepsilon}$$

(4)

where $C_\mu = 0.09$ is an empirical coefficient, k the turbulent kinetic energy and ε the dissipation rate of turbulent kinetic energy.

The k and ε values can be obtained from the following equations:

$$\frac{\partial(\rho k)}{\partial t} + \frac{\partial}{\partial x_i}(\rho U_j k) = \frac{\partial}{\partial x_i}\left[\left(\mu + \frac{\mu_t}{\sigma_k}\right)\frac{\partial k}{\partial x_j}\right] + P_k - \rho\varepsilon + P_{kb}$$

(5)

$$\frac{\partial(\rho\varepsilon)}{\partial t} + \frac{\partial}{\partial x_i}(\rho U_j \varepsilon) = \frac{\partial}{\partial x_i}\left[\left(\mu + \frac{\mu_t}{\sigma_\varepsilon}\right)\frac{\partial \varepsilon}{\partial x_j}\right] + \frac{\varepsilon}{k}\left(C_{1\varepsilon}P_k - C_{2\varepsilon}\rho\varepsilon + C_{1\varepsilon}P_{kb}\right)$$

(6)

$C_{1\varepsilon}$, $C_{2\varepsilon}$, σ_k and σ_ε are constants (1.44, 1.92, 1.0 y 1.3, respectively), P_k is the turbulence produced by viscous forces, while P_{kb} and $P_{\varepsilon b}$ represent the influence of the gravity forces.

In ANSYS CFX and OpenFOAM both phases, air and water, have been solved through an homogeneous model. Whereas in FLOW-3D free surfaces have been modeled with a simplified Volume of Fluid (VOF) technique (Hirt and Nichols [8]). Actually, only the water phase has been solved (FLOW Science Inc. [6]).

The model boundary conditions corresponded to the flow, the turbulence at the inlet condition, the upstream and downstream levels and their hydrostatic pressures distributions. In ANSYS CFX, the atmosphere condition has been simulated as an opening condition with a relative pressure of 0 Pa, air volume fraction of 1 and water volume fraction of 0.

Meshes have been compounded with hexahedral elements with a length scale of around 0.01 m.

The outlet condition has been considered as an opening condition with normal direction to the boundary condition and hydrostatic pressure. The water level height at outlet has been modified according to the water depth measured in the laboratory device. No slip conditions and smooth walls have been used as boundary condition in the walls.

Regarding the time-step, ANSYS CFX allows to use a fix time-step. Hence, a 0.05-second time-step was considered. In FLOW-3D, the timescale is obtained in each step in order to satisfy different internal stability criteria. The final time-step in the majority of the simulations was between 0.001 and 0.004 s. In OpenFOAM time step has been adjusted in order to keep Courant Number below 0.5, leading to time steps around 0.0002 and 0.00005 s.

In judging the convergence of a solution in a finite-volume scheme, a widely used method entails monitoring the residuals (Wasewar and Vijay Sarathi [13]). Residuals are defined as the imbalance in each conservation equation following each iteration. The solution is said to have

converged if the scaled residuals are smaller than prefixed values ranging between 10^{-3} and 10^{-6}. In this work, the residual values were set to 10^{-4} for all the variables in ANSYS CFX and 10^{-6} in OpenFOAM.

ANALYSYS OF RESULTS

Figure 3 shows the comparison of the mean velocity profiles obtained with the two CFD codes and measured with ADV and PIV in a free hydraulic jump. y is the depth, y_1 the initial (supercritical) depth, V the horizontal velocity, V_1 the horizontal velocity correspondent to y_1, and L the length of the hydraulic jump measured in the lab. In general, results are similar in the different sections of the free hydraulic jump.

In the ADV equipment used, in order to avoid flow perturbations measurement point is configured by default far of the tips. In this way, it is required a minimum water depth to measure. This disabled the measurement of the point what were 0.05 m below the free surface level. Therefore, in the first section ($L/4$) it was possible to get a single measure point with ADV.

In the second section ($2L/4$), there is a good agreement between the velocity profiles obtained from ANSYS CFX and FLOW-3D simulations and PIV and ADV measurements. Furthermore, similar profiles are obtained in the following sections ($3L/4$ and $4L/4$), although FLOW-3D tended to obtain higher velocities near the bottom. Despite the recirculation region is out of the available range of the equipment used in this work, numerical results seem to underestimate such region.
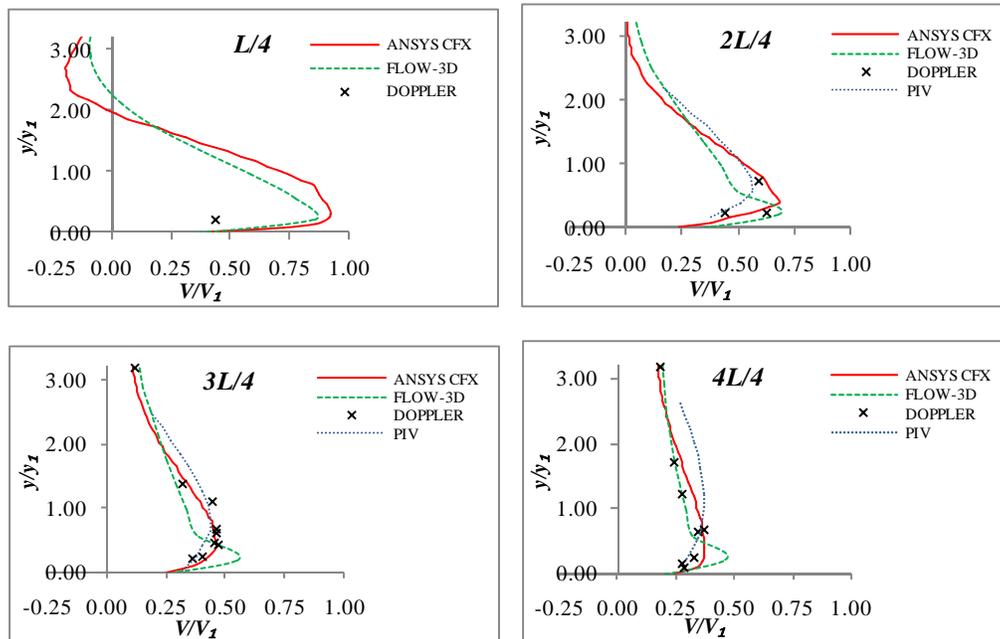

Figure 3. Profiles of mean velocity in different sections of the free hydraulic jump

Figure 4 shows the comparison of the mean velocity profiles obtained with the five methods in a submerged hydraulic jump. Results have been non-dimensioned by using the values of y_1 and V_1 of the corresponding free hydraulic jump.

Although the sluice gate has not been simulated in the CFD codes, results are close to ADV and PIV measurements. ANSYS CFX tends to overestimate the velocity in the second half of the submerged hydraulic jump (sections $3L/4$ and $4L/4$), while FLOW-3D tends to overestimate the velocity in the bottom. OpenFOAM results are closer to laboratory measures.
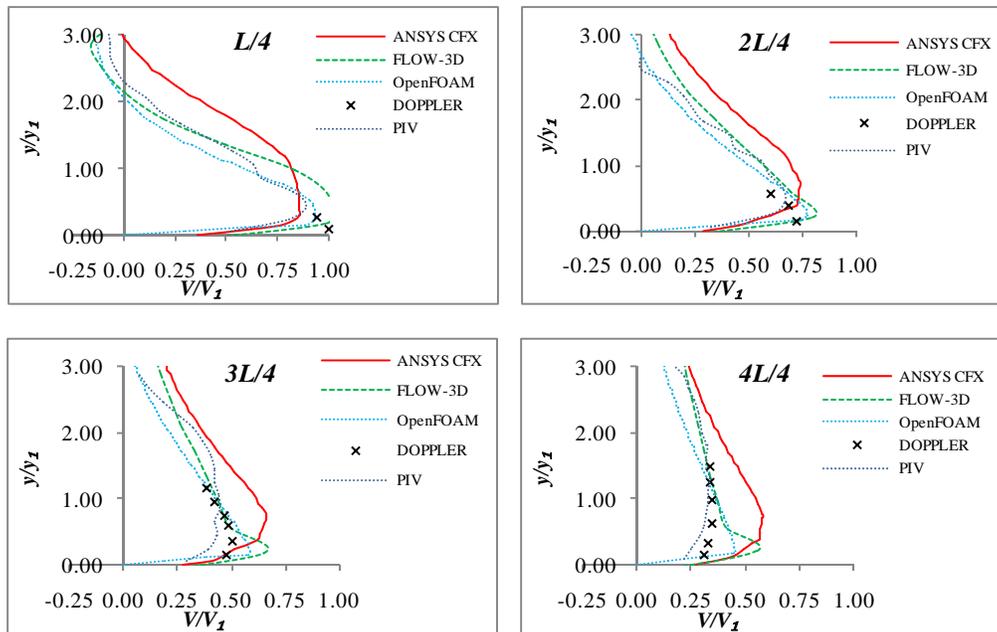
Figure 4. Profiles of mean velocity in different sections of the submerged hydraulic jump

Figures 5-7 shows the velocity vectors and the mixture of both fluids for the submerged hydraulic jump case. Qualitatively, CFD results show important air entrain in the first part of the jump as shown by previous studies. This is due to the recirculation of the flow that increases the turbulent kinetic energy, and consequently, air entrain in the water. However, the aeration does not reach the channel bottom with none of the CFD codes used.
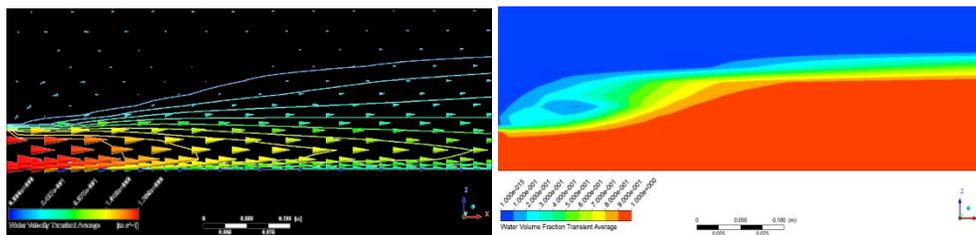

Figure 5.Velocity vectors and volume fraction in submerged hydraulic jump with ANSYS CFX
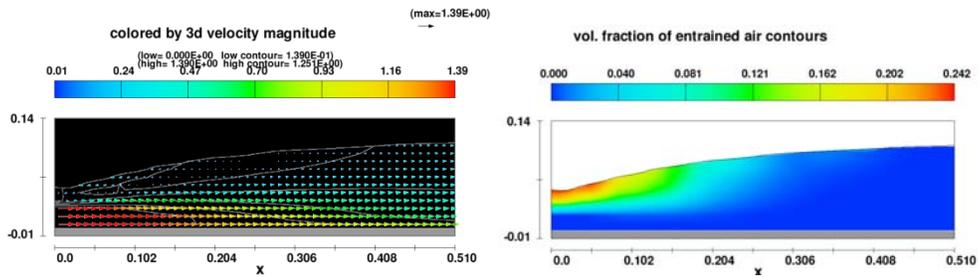
Figure 6. Velocity vectors and volume fraction in submerged hydraulic jump with FLOW-3D
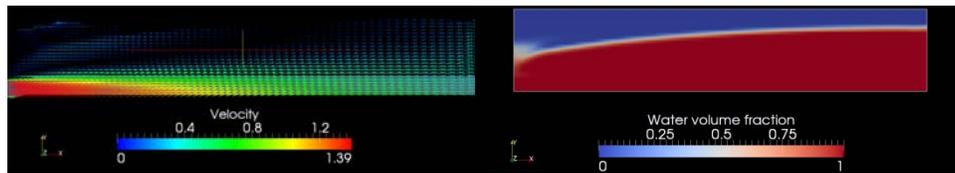

Figure 7. Velocity vectors and volume fraction in submerged hydraulic jump with OpenFOAM

CONCLUSIONS

In this work, two hydraulic jumps have been measured through ADV and PIV, whereas CFD simulations have been done by using three of the most widely used codes. With regard to the velocity profiles, simulations are quite similar to laboratory results. The results demonstrate the suitability of crossing methodologies to solve complex phenomena.

The paper is the first step to analyze the turbulent structure of a two-phase air-water flow in both, free and submerged, hydraulic jumps. Nevertheless, there has been found some difficulties to obtain reliable results in the recirculation area of the second half of the jumps. In fact, there are doubts about the suitability of using the k-ε turbulence model to solve hydraulic jumps. This model seem to fail in the accurate prediction of the recirculation region. Behavior of other turbulence models should be analyzed. For instance, in stilling basins where air entrain and recirculation phenomena are also present, k-ω turbulence models shows a better agreement than k-ε (Castillo *et al.* [4]). However, currently such models are not available in FLOW-3D. Moreover, air entrainment is going to be measured through a optical fiber equipment.

ACKNOWLEDGMENTS

REFERENCES

[1] ANSYS, Inc., "ANSYS CFX. Solver Theory Guide. Release 13.0.", (2010).

[2] Castillo, L. G., "Validation of instantaneous velocities measurements with ADV equipment in turbulent high two-phase flows", The Eight International Conference on Hydro-Science and Engineering (ICHE), Nagoya, Japan, (2008).

[3]   Castillo, L. G., *"Filtering and validation of velocities obtained with ADV equipment inside of hydraulic jumps", International Workshop on Environmental Hydraulics, IWHE, Valencia, Spain, (2009).*

[4]   Castillo, L. G., Carrillo, J. M., and Sordo-Ward, A., *"Simulation of overflow nappe impingement jets", Accepted for publication in the Journal of Hydroinformatics, (2014).*

[5]   Etalon Research Ltd., *"Manual for the rtCam PIV system. Version 1.3", (2009).*

[6]   FLOW Science, Inc., *"FLOW 3D. Theory v10.0", (2011).*

[7]   Harlow, F. H., and Nakayama, P. I., *"Transport of turbulence energy decay rate", Los Álamos Sci. Lab. University of California, (1968).*

[8]   Hirt, C. W., and Nichols, B. D., *"Volume of fluid (VOF) method for the dynamics of free boundaries", Journal of Computational Physics, Vol. 39, (1981) , pp 201-225.*

[9]   Launder, B. E., and Sharma, B. I., *"Application of the energy dissipation model of turbulence to the calculation of flow near a spinning disc", Heat and Mass Transfer, Vol. 1, No. 2, (1974) , pp 131-138.*

[10] Nortek AS, *"Nortek 10 MHz Velocimeter. Operations Manual", (2000).*

[11] OpenFOAM Foundation. *"OpenFOAM. The Open Source CFD Toolbox. User Guide", (2013).*

[12] Wasewar, L. and Vijay Sarathi, J., *"CFD modelling and simulation of jet mixed tanks" Eng. Appl. Comp. Fluid Mech. Vol. 2, No. 2, pp 155-171, (2008).*